

Combined Fast Reversible Liquid-like Elastic Deformation with Topological Phase Transition in Na_3Bi

Xiyue Cheng,¹ Ronghan Li,¹ Dianzhong Li,¹ Yiyi Li,¹ and Xing-Qiu Chen^{1,*}

¹Shenyang National Laboratory for Materials Science, Institute of Metal Research,
Chinese Academy of Science, 110016 Shenyang, Liaoning, China

(Dated: May 18, 2015)

By means of first-principles calculations, we identified the structural phase transition of Na_3Bi from hexagonal ground state to cubic $cF16$ phase above 0.8 GPa, in agreement with the experimental findings. Upon the releasing of pressure, $cF16$ phase of Na_3Bi is mechanically stable at ambient condition. The calculations revealed that the $cF16$ phase is topological semimetal, in similarity to well-known HgTe and it even exhibits an unusually low C' modulus (only about 1.9 GPa) and a huge anisotropy, A'' of as high as 11, the third highest value among all known cubic crystals in their elastic behaviors. These facts render $cF16$ -type Na_3Bi very soft with a liquid-like elastic deformation in the $(110)\langle\bar{1}\bar{1}0\rangle$ slip system. Importantly, as accompanied with this deformation, Na_3Bi shows a topological phase transition from a topological semimetal state at its strain-free cubic phase to a topological insulating state at its distorted phase. Because the C' elastic deformation almost costs no energy in a reversible and liquid-like soft manner, $cF16$ -type Na_3Bi would potentially provide a fast on/off switching way between topological insulator and topological semimetal, which would be beneficial to the quantum electronic devices for practical applications.

PACS numbers: 71.70.Ej, 73.20.At, 62.20.Dc

The topological material have been extensively studied and its number and types have increased dramatically over the past decades. As the first member of the topological family, the topological insulators (TIs) are materials with a bulk band gap but have protected metallic states on their edge/surface, originating from the combination of spin-orbit interactions and time-reversal symmetry[1–3], including Bi_2Se_3 [4, 5] and the topological crystalline insulators (TCIs) such as $\text{Pb}_{1-x}\text{Sn}_x\text{Te}(\text{Se})$, SnSe , and SnS [6–8]. In analogy to TIs, the non-trivial topology of the band structure in semimetal gives rise to other new states of matters, topological Dirac semimetals (TDSs) and topological Weyl semimetals (TWSs). For both TDSs and TWSs, the bulk conduction and valence bands touch only at discrete (Dirac) points and disperse linearly along all momentum directions, while their low-energy bulk excitations are described by the Dirac and Weyl equations, respectively. Compared to Dirac semimetal, inversion or time reversal symmetry must be broken in Weyl semimetal. For example, Na_3Bi [9–12] and Cd_3As_2 [13–15] were theoretically and experimentally demonstrated to be 3D TDSs protected by crystal symmetry and the noncentrosymmetric materials including TaAs, TaP, NbAs, and NbP [16] was recently predicted as natural TWSs. Certainly, the topological concept can be also introduced into metals leading to topological metals (TMs). Generally, most of TMs can be manually achieved from TIs or semimetals, yet so far several compounds, such as HgTe [17, 18] and NaBi [20], were found to be a native 3D TM. Although the flourishing topological material has inspired great interest, one has to admit the fact that some existed challenges are restricting its development, no matter from the aspects of scientific researches or technological application.

Besides two often facing challenges (small band gap and small quantized conductance of the edge state) [4, 5, 18, 19],

another main challenge is the lacking of effective ways [19] to control the phase transition between topological materials and regular insulators or metals. Traditionally, the control of topological phase transitions was realized mainly by pressure, lattice strain, or chemical substitution. For instance, $hP8$ -type Na_3Bi undergoes a topological phase transition from a Dirac semimetal to a trivial insulator upon doping Sb or P through varying the concentrations of $\text{Na}_3\text{Bi}_{1-x}(\text{Sb},\text{P})_x$ [21]. However, via such a way it is extremely difficult to make the transition reversible once the material is fabricated. But, is there any way to rapidly and effectively switch on or off these phase transitions, rather than traditional means? This definitely poses a challenging issue.

As advanced functional materials, the elastic or mechanical properties of topological materials were often neglected and concealed under their wonderful and shining electronic properties. It is true that a vast majority of topological materials only have ordinary elastic or mechanical properties which may just indicate the structural mechanical stability [22]. Thus, it would be highly interesting to find a topological material with extinct elastic or mechanical properties. Recently, Na_3Bi was proposed and demonstrated to be a 3D TDS [9–12], and it is found that Na_3Bi would undergo a structural phase transition of from its hexagonal ground state ($hP24$) to a cubic $cF16$ phase at 0.8 GPa [23], in well agreement with the experimental findings [24–26]. To one's surprise, this $cF16$ - Na_3Bi exhibits an unusually low C' modulus (only about 1.9 GPa) and a huge anisotropy, A'' of as high as 11, the third highest value among all known cubic crystals in its elastic properties. These facts render $cF16$ -type Na_3Bi very soft with a liquid-like elastic deformation in the $(110)\langle\bar{1}\bar{1}0\rangle$ slip system. Meanwhile, as the C' elastic deformation induced a topological phase transition from TS to TI and it almost cost no energy in a reversible and liquid-like elastic manner, this cubic Na_3Bi

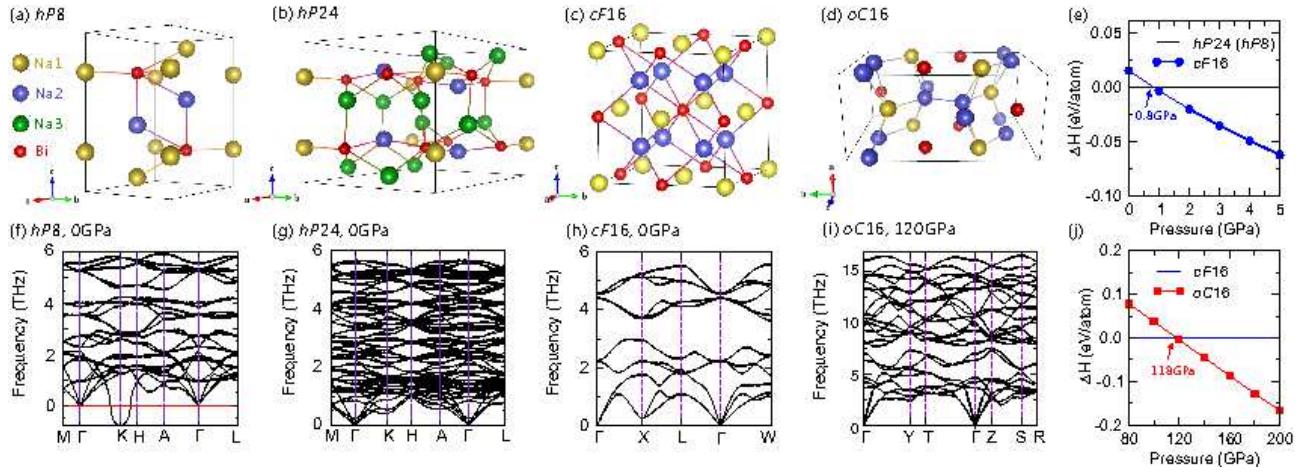


FIG. 1: (Color online) The DFT-derived pressure-dependent phase transitions of Na_3Bi . (a) $hP8$ hexagonal phase, which was experimentally claimed to be stable at the ground state under ambient pressure, (b) $hP24$ hexagonal phase, which was theoretically found to be stable at the ground state under ambient pressure, (c) $cF16$ cubic phase, which is more stable in energy above 0.8 GPa than both $hP8$ and $hP24$ phases, and (d) $oC16$ orthorhombic phase, which is more stable above 118 GPa. (f,g,h,i) the derived phonon dispersions of $hP8$ (0 GPa), $hP24$ (0 GPa), $cF16$ (0 GPa) and $oC16$ (120 GPa), respectively. (e and j) the pressure-dependent enthalpies of $hP8$, $hP24$, $cF16$ and $oC16$ phases to show the pressures of phase transitions. The red circles represent the Bi atoms while the Na atoms are shown in different color according to their Wyckoff sites. Here, yellow, blue and green circles represents Na1, Na2 and Na3 atoms, respectively.

phase would potentially provide a fast on/off switching way between TI and TS.

The structural optimization, electronic properties and elastic behaviors of the Na_3Bi phases were calculated within the framework of density functional theory (DFT) [27, 28] using the Vienna *ab initio* Simulation Package (VASP) [29, 30] with the projector augmented wave (PAW) method [31] and generalized gradient approximation (GGA) within the Perdew-Burke-Ernzerhof (PBE) exchange-correlation functional [32]. The cutoff energy for the expansion of the wavefunction into plane waves was set at 350 eV and the tetrahedron method with Blöchl corrections was utilized. All the Brillouin zone integrations were performed on Monkhorst-Pack k -meshes and was sampled with a resolution of $2\pi \times 0.07 \text{ \AA}^{-1}$, which showed excellent convergence of the energy differences and stress tensors. For hexagonal structures, the Brillouin zone integrations were performed on the Γ -centered symmetry. To check the dynamical stability, we further derived the phonon dispersion curves using the finite-displacement approach as implemented in the *Phonopy* code [33]. The phonon frequencies are constructed from forces, resulting from displacements of certain atoms in a supercell containing typically 80-100 atoms for each Na_3Bi phases, respectively. The electronic localized function (ELF)[34–36] was done using the grid-based algorithm with $100 \times 100 \times 100$ grids. In addition, all crystal structures and ELF diagrams were generated using VESTA [37].

The latest discoveries that native Na_3Bi is a three dimensional (3D) Dirac semimetal represent a significant advance in topological Dirac materials [9–11], because this material enables the study of a new type of quantum state. At ambient condition, Na_3Bi possesses bulk Dirac fermions in 3D at

the Fermi level, which disperse linearly along all three momentum directions [9, 11], in contrast to the two-dimensional Dirac fermions present on the surfaces of 3D topological insulators and in graphene [38].

Recently, the first-principles calculations revealed that the previously experimentally characterized $hP8$ phase (Fig. 1a) is unstable at the ground state due to the presence of a negative phonon branch around the high-symmetry X point, as illustrated in Fig. 1(f). Instead, the calculation suggested that the real ground-state phase would be the $hP24$ phase (Fig. 1(b)), which is indeed a distorted superlattice version of the $hP8$ phase [11]. Importantly, this stable $hP24$ structure exhibits a semblable 3D TDS feature as what the $hP8$ phase presents [9].

Furthermore, the previous experiments demonstrated that Na_3Bi undergoes a phase transition above the pressures of 0.7-1.0 GPa[24–26]. In nice agreement with the experimental measurements, our first-principles calculations successfully reproduced this phase transition from the ground-state $hP24$ (or $hP8$) phase to the cubic $cF16$ phase (Fig. 1(c)) above 0.8 GPa [23], as shown in Fig. 1(e). The calculations demonstrated that, even upon the releasing pressure, the $cF16$ phase is still mechanically and dynamically stable at zero pressure, as elucidated by its phonon dispersions (Fig. 1(h)). This fact indicates that the $cF16$ -type phase is quenchable at ambient condition once it is synthesized above 0.8 GPa. Specifically, this cubic Na_3Bi crystalizes in a BiF_3 -type structure (space group of $Fm\bar{3}m$) with $a=7.550 \text{ \AA}$ at ambient zero pressure. The Bi atoms lie at $4b$ site (0.5, 0.5, 0.5) and the Na atoms occupy two inequivalent sites, $4a$ (0, 0, 0) and $8c$ (3/4, 3/4, 3/4). The calculation also revealed that, by further increasing the pressure up to above 118 GPa, the cubic $cF16$ phase can

be transformed into an orthorhombic $oC16$ phase (Fig. 1(d) and Fig. 1(j)), which is a wide-gap insulator [23].

Surprisingly, this cubic $cF16$ phase exhibits several unusual elastic behaviors in its mechanical properties. At 0 GPa, the DFT-derived single crystal elastic constants are $C_{11} = 22.3$ GPa, $C_{12} = 18.4$ GPa and $C_{44} = 21.9$ GPa. Firstly, C_{11} is very close to C_{44} , which gives nearly coinciding longitudinal and transverse acoustic phonons along the direction of $\langle 001 \rangle$. This fact is reflected well by that two phonon branches along this Γ -X direction (Fig. 1(h)) are nearly degenerated at small q values close to the Γ point. Secondly, it has been noted that the difference of $C_{44}-C_{12}$ is only about 3.5 GPa, revealing a very small deviation from the Cauchy relation with $C_{44} = C_{12}$, which measures the importance of the angular dependence in atomic forces as compared to the central force description. Thirdly, $cF16$ - Na_3Bi has a rather low $C' = \frac{C_{11}-C_{12}}{2} = 1.9$ GPa. Note that C' represents the resistance to shear deformation by a shear stress applied across the (110) plane in the $\langle 1\bar{1}0 \rangle$ direction and it indeed measures the rigidity against the volume-conserving tetragonal deformation. We further derived its universal anisotropic ratio to be as high as $A'' = 11.07$, according to the recently proposed definition of the universal elastic anisotropy index [39], highlighting a huge anisotropy in its elastic properties. Furthermore, we plot the C' versus A'' for a variety of cubic crystals (330 compounds, elastic data from the supplementary table of ref. [40]) as illustrated in Fig. 2(a and b). Among those compounds, we have observed from the plot that the cubic Na_3Bi almost exhibits the lowest C' value and the third highest anisotropic ratio A'' (which are only lower than two known superelastic compounds of CuZn and CuAuZn_2)[41, 42]. These unique features render $cF16$ - Na_3Bi special: it is very soft, showing a liquid-like behaviour along the C' deformation corresponding to the shear slip $(110)\langle 1\bar{1}0 \rangle$ system within the elastic regime. This fact has also been evidenced by Fig. 2(c), from which it can be seen that the C' deformation almost costs no energy, based on the deformation energy-versus-strain relation. In particular, it has been also found that, the C' and universal anisotropic ratio A'' show unusual trends with increasing pressure, as evidenced in Fig. 2(d). In the first range below 1 GPa, both C' and A'' remain almost constant and, in the pressure range from 1 GPa to 4 GPa C' rapidly increases from 2 GPa to 6 GPa whereas A'' shows an apparent drop from about 11 to 6. Above about 4 GPa, they again almost become constant. In particular, the liquid-like and soft elastic behavior of Na_3Bi remains robust in a certain pressure range at least from 0 GPa to 1 GPa.

Importantly, the huge anisotropic ratio of $cF16$ -type Na_3Bi has been further reflected by the stereographic projections at ambient pressure in Fig. 3(a and c), which are used in order to show the particular crystal orientation and the corresponding Young's and shear moduli more clearly, while the 3D representation surfaces (Fig. 3(b and d)) visualized the crystallographic-orientation dependent Young's and shear moduli which, however, presents the strong and weak directions in one crystal structure directly[43]. Note that the neg-

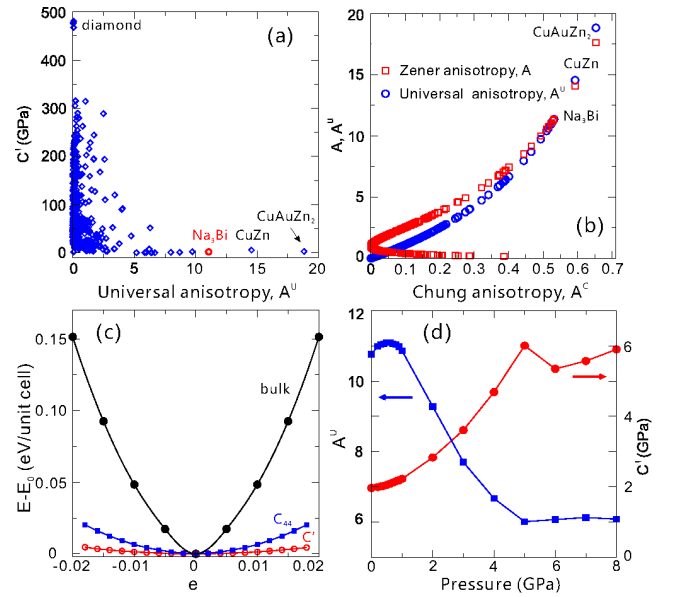


FIG. 2: (Color online) The liquid-like elastic behavior of Na_3Bi . (a) C' versus universal anisotropic ratio A'' , showing that Na_3Bi has an extremely low C' and a highly large A'' among a variety of cubic crystals, (b) anisotropic ratio A'' versus Chung anisotropy A^c for a variety of cubic crystals, (c) the DFT-derived deformation energy as a functional of strain according to the definition of elastic energies of bulk modulus, C_{44} , and C' at 0 GPa, (d) the pressure-dependent universal anisotropic ratio A'' and C' .

ative sign only denotes the negative direction corresponding to the positive one. In its stereographic projections, each blue point denotes one crystal orientation and the lines with different colour and density represent the counter lines of Young's or shear moduli. It can be seen that the elastic properties under different crystal orientations highly vary from each other. For Young's modulus, the lowest and highest orientations are $[001]$ ($E_{[001]} = 6.42$ GPa) and $[111]$ ($E_{[111]} = 53.9$ GPa), respectively. In contrast, its shear modulus exhibits an opposite trend. The $[001]$ orientation has the highest shear modulus of $G_{[001]} = 24.5$ GPa and the $[111]$ one with the lowest value of $G_{[111]} = 3.17$ GPa. There is no doubt that their opposite trends between both $[001]$ and $[111]$ directions substantially contribute to the huge anisotropy of this cubic crystal. Mechanically, the huge anisotropy can be attributed to the electronic structures and atomic arrangements. As illustrated in the electronic localization function (ELF) images (Fig. 3(e,f,g)), the (001) plane consists of Bi and Na atoms within the ionic-bonding manner (Fig. 3(e)), whereas the (111) plane is indeed comprised by the densest metallic Na atoms with pure metallic bonds (Fig. 3(g)). It is clear that the dense (111) plane is hard to be compressed, but it can be easily sheared under deformation due to the pure metallic bonds. However, for the (001) plane, all bonds are ionic Na-Bi bonds with low atomic density. This interprets as to why the resistance to the compression of the (001) plane is low, whereas its shear modulus is much higher. Similar interpretation also holds for the (110)

plane (Fig. 3(f)), from which we can see that both Na-Na metallic bonds and Na-Bi ionic bonds co-exist (*c.f.* and the metallic bonds form a pure channel along the $\langle 110 \rangle$ direction, Fig. 3(f), leading to the intermediate Young's and shear moduli.

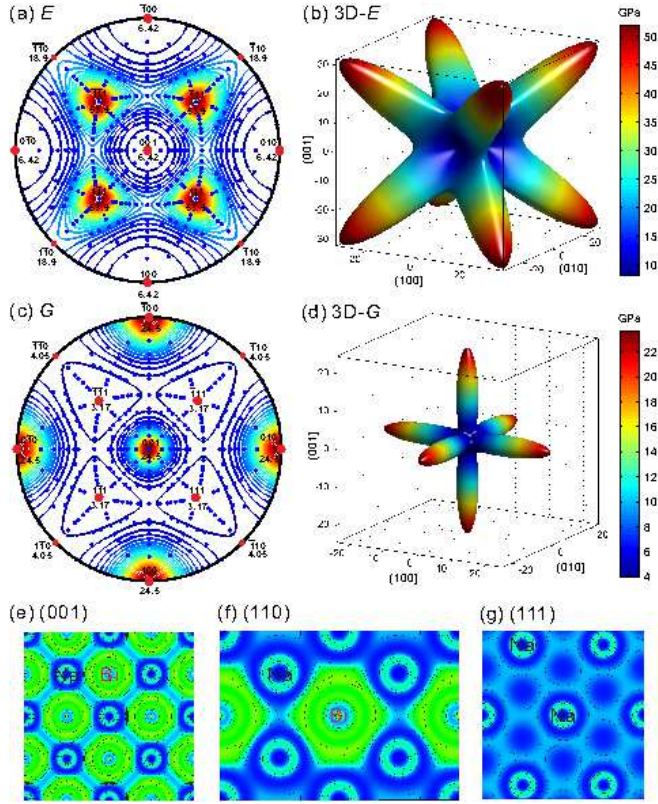


FIG. 3: (Color online) Huge elastic anisotropy of Na_3Bi . (a and c) The stereographic projections of the Young's and shear moduli, respectively. (b and d) The representation surfaces for the crystallographic-orientation depended Young's and shear moduli, respectively. (e, f, and g) The electron localization function (ELF) isosurface maps for the (001), (110) and (111) planes, respectively.

In addition to its unusual elastic properties, the cubic $cF16$ phase of Na_3Bi exhibits another type of attractive electronic properties, in different from the ground-state $hP24$ phase with unique feature of 3D TDS. From Fig. 4(a), it has been seen that the Fermi level exactly crosses the threefold degenerated Bi- $p_{(x,y,z)}$ states (Γ_4) at Γ for $cF16$ -type Na_3Bi at 0 GPa. If the spin-orbit coupling (SOC) effect is included, this threefold degenerated Γ_4 p -states would further split into the doubly degenerated $|p_{\frac{3}{2}}\rangle$ and nondegenerated $|p_{\frac{1}{2}}\rangle$ states, as shown in Fig. 4(c). With this electronic feature, it is clear that in the strain-free cubic case Na_3Bi is a semimetal because its conduction and valence bands touch only at the Γ point. Another typical feature is that even in the case without SOC, the Na- $3s$ states (Γ_1) are energetically lower by about 0.4 eV than the Bi- $6p$ states (Γ_4) at the Γ point (Fig. 4(a)). More importantly, Γ_1 and Γ_4 exhibits the opposite parities. However, it is worth noting that no any other band inversions present for the rest high symmetric points in the BZ. These facts imply that

Na_3Bi naturally processes the inverted band ordering, which is a prerequisite for the occurrence of topological electronic properties. Interestingly, when the SOC is switch on, the inverted band ordering is further enhanced. The Na- $3s$ state (Γ_6^+ in Fig. 4(c)) is significantly reduced in energy by increasing the energy difference up to 0.74 eV (Fig. 4(c)). Therefore, in its strain-free cubic case, $cF16$ - Na_3Bi is a TS at 0 GPa, no matter whether the spin-orbit coupling effect (SOC) is considered. Note that this topological semimetal feature of $cF16$ - Na_3Bi remains unchanged up to 3.65 GPa before it transforms to a regular insulator [23]. Certainly, it needs to be emphasized that the band inversion at Γ is caused by the crystal field effect via the protection of lattice symmetry, rather than the chemical doping, pressure or strains. This feature is similar to the famous case of HgTe with a nearly zero direct band gap at Γ point in the BZ and an analogous inverted band ordering [17].

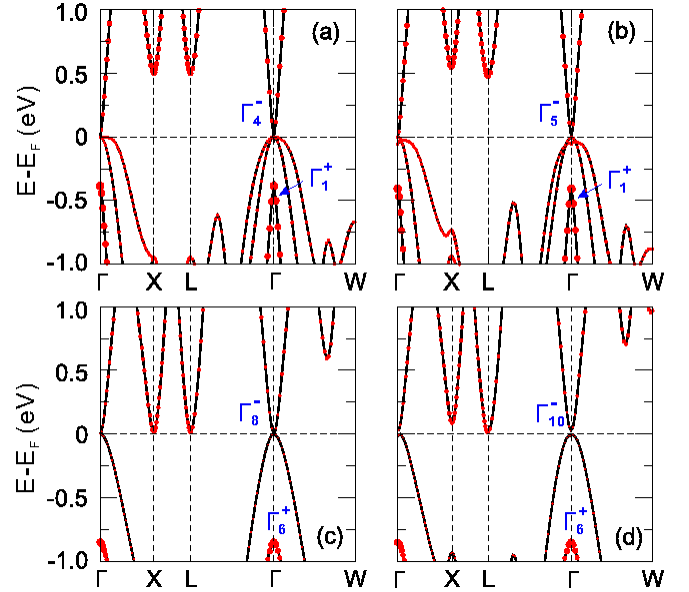


FIG. 4: (Color online) Topological phase transition from topological semimetal to topological insulator under the C' tetragonal deformation. Band structures for cubic $cF16$ -type Na_3Bi (a and c) and for its distorted structure via the C' deformation with a 4% strain (b and d). a and b: no SOC inclusion; c and d: with SOC inclusion. The solid circles denote the s -like states.

The doubly degenerated $|p_{\frac{3}{2}}\rangle$ states crossing the Fermi level in Fig. 4(c) can be certainly broken by the engineering of strains. Importantly, via the liquid-like C' soft deformation of the $(110)\langle 1\bar{1}0 \rangle$ slip system, our calculation demonstrated that the $cF16$ - Na_3Bi can be indeed transformed into a TI from its intrinsic feature of a TS. From Fig. 4(b and d) the band structure at around the Fermi level depends sensitively on the lattice distortion along the soft $(110)\langle 1\bar{1}0 \rangle$ tetragonal elastic distortion. Without the SOC inclusion any slight lattice distortion along the C' deformation breaks up the triply degenerated Bi- $p_{(x,y,z)}$ states (Γ_4) at Γ into doubly degenerated Bi- $p_{x,y}$ and nondegenerated Bi- p_z states (see Fig. 4(b) with

a 4% distortion). Furthermore, with the SOC inclusion, the doubly degenerated Bi- $p_{x,y}$ states at the Fermi level is further broken to open a band gap, as evidenced in Fig. 4(d). In the meanwhile, such a distortion does not affect its band inversion. From Fig. 4(d), the nondegenerated Na-3s state (Γ_6^+) is energetically lower by about 0.76 eV than the Bi- p state (Γ_{10}^-) at the Γ point. It needs to be emphasized that for cubic structure the product of the parities of the Bloch wave function for the occupied bands at time-reversal invariant momenta (TRIMs) of three equivalent X (0.5,0,0), three equivalent M (0.5,0.5,0), and single R (0.5,0.5,0.5) has been derived to be -1, whereas at Γ it is +1. Via the C' deformation, although that these three equivalent momenta of X (or M) can be lifted, the product of the parities for all occupied bands at the TRIMs of Γ , R, X and M still remains -1. Therefore, these results evidence that the distorted cubic Na₃Bi by the strain engineering along the C' deformation is a three-dimensional topological insulator. Importantly, because of the reversible liquid-like elastic behavior along the C' deformation which almost cost no energy, the $cF16$ -type Na₃Bi becomes a highly attractive compound. Through such a way, one would easily realize rapid on/off switching from a TS state in its cubic phase to a TI state in its distorted lattice.

In summary, we have demonstrated that a soft liquid-like elastic control of topological phase transition in cubic $cF16$ -type Na₃Bi can be achieved through the C' tetragonal deformation along the (110) $\langle 1\bar{1}0 \rangle$ slip system, highlighting a realization of a fast and reversible on/off switching way between topological semimetal and topological insulator. This would be beneficial to the quantum electronic devices for practical applications.

Acknowledgments This work was supported by the "Hundred Talents Project" of the Chinese Academy of Sciences and by the Key Research Program of Chinese Academy of Sciences (Grant No. KGZD-EW-T06) and NSFC of China (Grand Numbers: 51074151). The computational resource is using the local HPC cluster of the Materials Process Modeling Division in the IMR as well as the National Supercomputing Center in Tianjin (TH-1A system).

* Corresponding author: xingqiu.chen@imr.ac.cn

- [1] M. Z. Hasan and C. L. Kane, Rev. Mod. Phys. **82**, 3045 (2010).
 [2] X.-L. Qi and S.-C. Zhang, Rev. Mod. Phys. **83**, 1057 (2011).
 [3] B. Yan and S. C. Zhang, Rep. Prog. Phys. **75**, 096501 (2012).
 [4] H. Zhang, C.-X. Liu, X.-L. Qi, X. Dai, Z. Fang and S.-C. Zhang, Nat. Phys., **5**, 438 (2009).
 [5] Y. Xia, D. Qian, D. Hsieh, L. Wray, A. Pal, H. Lin, A. Bansil, D. Grauer, Y. S. Hor, R. J. Cava and M. Z. Hasan, Nat. Phys. **5**, 398 (2009).
 [6] T. H. Hsieh, H. Lin, J. Liu, W. Duan, A. Bansil and L. Fu, Nat. Commun. **3**, 982 (2013).
 [7] S. Y. Xu, C. Liu, N. Alidoust, M. Neupane, D. Qian, I. Belopolski, J. D. Denlinger, Y. J. Wang, H. Lin, L. A. Wray, G. Landolt, B. Slomski, J. H. Dil, A. Marcinkova, E. Morosan, Q. Gibson, R. Sankar, F. C. Chou, R. J. Cava, A. Bansil and M. Z. Hasan, Nat. Commun. **3**, 1192 (2013).
 [8] Y. Sun, Z.C. Zhong, T. Shirakawa, C. Franchini, D. Z. Li, Y.Y. Li, S. Yunoki, and X.-Q. Chen, Phys. Rev. B **88**, 235122 (2013).
 [9] Z. Wang, Y. Sun, X.-Q. Chen, C. Franchini, G. Xu, H. Weng, X. Dai, and Z. Fang, Phys. Rev. B **85**, 205101 (2012).
 [10] Z. K. Liu, B. Zhou, Y. Zhang, Z. J. Wang, H. M. Weng, D. Prabhakaran, S.-K. Mo, Z. X. Shen, Z. Fang, X. Dai, Z. Hussain, and Y. L. Chen, Science **343**, 864 (2014).
 [11] X. Y. Cheng, R. H. Li, X.-Q. Chen, D. Z. Li, and Y. Y. Li, Phys. Rev. B **89**, 245201 (2014).
 [12] S. Y. Xu, C. Liu, S. K. Kushwaha, R. Sankar, J. W. Krizan, I. Belopolski, M. Neupane, G. Bian, N. Alidoust, T.-R. Chang, H.-T. Jeng, C.-Y. Huang, W.-F. Tsai, H. Lin, P. P. Shibayev, F.-C. Chou, R. J. Cava and M. Z. Hasan, Science **347**, 294 (2015).
 [13] Z. Wang, H. Weng, Q. Wu, X. Dai, and Z. Fang, Phys. Rev. B **88**, 125427 (2013).
 [14] M. N. Ali, Q. Gibson, S. Jeon, B. B. Zhou, A. Yazdani and R. J. Cava, Inorg. Chem. **53**, 4062 (2014).
 [15] Z. K. Liu, J. Jiang, B. Zhou, Z. J. Wang, Y. Zhang, H. M. Weng, D. Prabhakaran, S. K. Mo, H. Peng, P. Dudin, T. Kim, M. Hoesch, Z. Fang, X. Dai, Z. X. Shen, D. L. Feng, Z. Hussain and Y. L. Chen, Nat. Mater. **13**, 677 (2014).
 [16] H. Weng, C. Fang, Z. Fang, A. Bernevig and X. Dai, Phys. Rev. X **5**, 011029 (2015).
 [17] B. A. Bernevig, T. L. Hughes and S. C. Zhang, Science **314**, 1757 (2006).
 [18] M. Konig, S. Wiedmann, C. Brune, A. Roth, H. Buhmann, L. Wiedmann, X. L. Qi and S. C. Zhang, Science, **318**, 766 (2007).
 [19] X. F. Qian, J. W. Liu, L. Fu and J. Li, Science, **346**, 1344 (2014).
 [20] R. H. Li, X. Y. Cheng, Q. Xie, Y. Sun, D. Z. Li, Y. Y. Li and X.-Q. Chen, Sci. Rep., **5**, 8446 (2015).
 [21] A. Narayan, D. Disante, S. Picozzi, and S. Sanvito, Phys. Rev. Lett., **113**, 256403 (2014).
 [22] B. Sa, J. Zhou, R. Ahuja and Z. Sun, Comput. Mater. Sci. **82**, 66 (2014).
 [23] X. Y. Cheng, R. H. Li, D. Z. Li, Y. Y. Li and X.-Q. Chen, Phys. Chem. Chem. Phys. **17**, 6933 (2015).
 [24] M. E. Leonova, S. A. Kulinich, and L. G. Sevast'yanova, Exp. Geosci. **7**, 55 (1998).
 [25] M.E. Leonova, I. K. Bdikin, S.A. Kulinich, O.K. Gulish, L.G. Sevast'yanova, K.P. Burdina, Inorg. Mater. **39**, 266 (2003).
 [26] S. A. Kulinich, M. E. Leonova, and L. G. Sevast'yanova, Zh. Obshch. Khim. **69**, 681 (1999).
 [27] P. Hohenberg, Phys. Rev. B **136**, 864 (1964).
 [28] W. Kohn and L. J. Sham, Phys. Rev. A **140**, 1133 (1965).
 [29] G. Kresse and J. Hafner, Phys. Rev. B **47**, 558 (1993).
 [30] G. Kresse and J. Furthmüller, Phys. Rev. B **54**, 11169 (1996).
 [31] P. E. Blöchl, Phys. Rev. B **50**, 17953 (1994).
 [32] J. P. Perdew, K. Burke, and M. Ernzerhof, Phys. Rev. Lett. **77**, 3865 (1996).
 [33] A. Togo, F. Oba, I. Tanaka, Phys. Rev. B **78**, 134106 (2008).
 [34] A. D. Becke and K. E. Edgecombe, J Chem. Phys. **92**, 5397 (1990).
 [35] B. Silvi and A. Savin, Nature **371**, 683 (1994).
 [36] A. Savin, R. Nesper, S. Wengert, and T. F. Fässler, Angew. Chem. Int. Ed. Engl. **36**, 1808 (1977).
 [37] K. Momma and F. Izumi, J. Appl. Crystallogr. **44**, 1272 (2011).
 [38] A. H. Castro Neto, N. M. R. Peres, K. S. Novoselov and A. K. Geim, Rev. Mod. Phys., **81**, 109 (2009).
 [39] S. I. Ranganathan and M. Ostojia-Starzewski, Phys. Rev. Lett., **101**, 055504 (2008).
 [40] H. Niu, X.-Q. Chen, P. Liu, W. Xing, X. Cheng, D. Li and Y. Li, Sci. Rep. **2**, 718 (2012).

- [41] G. M. McManus, Phys. Rev. **129**, 2004 (1963).
- [42] M. Meyers and K. K. Chawla, in *Mechanical Behavior of Materials*, Cambridge University Press, (2009).
- [43] X. Y. Cheng, X.-Q. Chen, D. Z. Li and Y. Y. Li, Acta Crystallogr. C Struct. Chem. **70**, 85 (2014).